The Kinetics of the Hydrogen/Deuterium Exchange of Epidermal Growth Factor Receptor Ligands

Ibon Iloro,* Daniel Narváez,* Nancy Guillén,[†] Carlos M. Camacho,[†] Lalisse Guillén,[†] Elsa Cora,*[‡] and Belinda Pastrana-Ríos*[†]

*Center for Protein Structure Function and Dynamics, and [†]Department of Chemistry, University of Puerto Rico, Mayagüez Campus, Mayagüez, Puerto Rico 00681-9019; and [‡]Department of Biochemistry, University of Puerto Rico, Medical Sciences Campus, San Juan, Puerto Rico 00936-5067

ABSTRACT   Five highly homologous epidermal growth factor receptor ligands were studied by mass spectral analysis, hydrogen/deuterium (H/D) exchange via attenuated total reflectance Fourier transform-infrared spectroscopy, and two-dimensional correlation analysis. These studies were performed to determine the order of events during the exchange process, the extent of H/D exchange, and associated kinetics of exchange for a comparative analysis of these ligands. Furthermore, the secondary structure composition of amphiregulin (AR) and heparin-binding-epidermal growth factor (HB-EGF) was determined. All ligands were found to have similar contributions of 3_{10}-helix and random coil with varying contributions of β-sheets and β-turns. The extent of exchange was 40%, 65%, 55%, 65%, and 98% for EGF, transforming growth factor-α (TGF-α), AR, HB-EGF, and epiregulin (ER), respectively. The rate constants were determined and classified as fast, intermediate, and slow: for EGF the 0.20 min^{-1} (Tyr), 0.09 min^{-1} (Arg, β-turns), and 1.88 $\times$ 10^{-3} min^{-1} (β-sheets and 3_{10}-helix); and for TGF-α 0.91 min^{-1} (Tyr), 0.27 min^{-1} (Arg, β-turns), and 1.41 $\times$ 10^{-4} min^{-1} (β-sheets). The time constants for AR 0.47 min^{-1} (Tyr), 0.04 min^{-1} (Arg), and 1.00 $\times$ 10^{-4} min^{-1} (buried 3_{10}-helix, β-turns, and β-sheets); for HB-EGF 0.89 min^{-1} (Tyr), 0.14 min^{-1} (Arg and 3_{10}-helix), and 1.00 x 10^{-3} min^{-1} (buried 3_{10}-helix, β-sheets, and β-turns); and for epiregulin 0.16 min^{-1} (Tyr), 0.03 min^{-1} (Arg), and 1.00 x 10^{-4} min^{-1} (3_{10}-helix and β-sheets). These results provide essential information toward understanding secondary structure, H/D exchange kinetics, and solvation of these epidermal growth factor receptor ligands in their unbound state.

INTRODUCTION

There are at least eight different epidermal growth factor receptor (EGFR) ligands, most of which are synthesized by the cell as transmembrane precursors that can be proteolytically cleaved and released to the extracellular matrix as soluble ligands which interact with the receptor (1). This interaction is a prerequisite step for the activation of the receptor and is followed by receptor dimerization and autophosphorylation, which in turn activate the microtubule-associated protein kinase pathway, leading to the signaling cascade which regulates cell differentiation, progression, and/or migration. The mechanism by which ligand binding occurs is summarized elsewhere (2–5). Lenferink (6) suggested that signal differentiation within the ErbB (i.e., EGFR) network occurs not only as a result of receptor differential expression but also as a result of different ligands activating the same receptor with different potencies. In this article, we present a comparative analysis for five of the eight EGFR ligands in terms of their conformation, hydrogen/deuterium (H/D) exchange kinetics, and extent of exchange based on Fourier transform-infrared (FT-IR) and two-dimensional correlation spectroscopy (2DCOS) and the oligomeric state of these ligands via mass spectrometry (MS). This information is essential to understanding the structure solvent accessibility hydrogen-bonding relationship of these ligands in their unbound state.

Amphiregulin (AR), whose structure has not yet been elucidated, and heparin binding-epidermal growth factor (HB-EGF) are ligands of the EGFR that are known to stimulate cell growth and proliferation and are often associated with oncogenesis (7–10). Amphiregulin, composed of 98 amino acids, and HB-EGF, composed of 86 residues (secondary structure composition is discussed herein), share a significant homology to all EGF family members containing an EGF-like domain (11,12) (Fig. 1) and share the same heparin-binding affinity (10,13). Recently discovered epiregulin (ER) (14), composed of 47 residues, is a ligand for EGFR and ErbB4, which also shares more than 41% amino acid sequence identity with EGF. ER exhibits the bifunctional regulatory property of inhibiting the growth of several epithelial cell lines while stimulating the growth of fibroblasts and various other cell types (8,15,16).

EGFR has a lower affinity for ER compared to EGF, AR, and HB-EGF (17), suggesting that EGFR is not the primary receptor for ER. Transforming growth factor-α (TGF-α) (18) is a mitogenic protein found in serum that is known to stimulate the growth of microvascular endothelial cells and
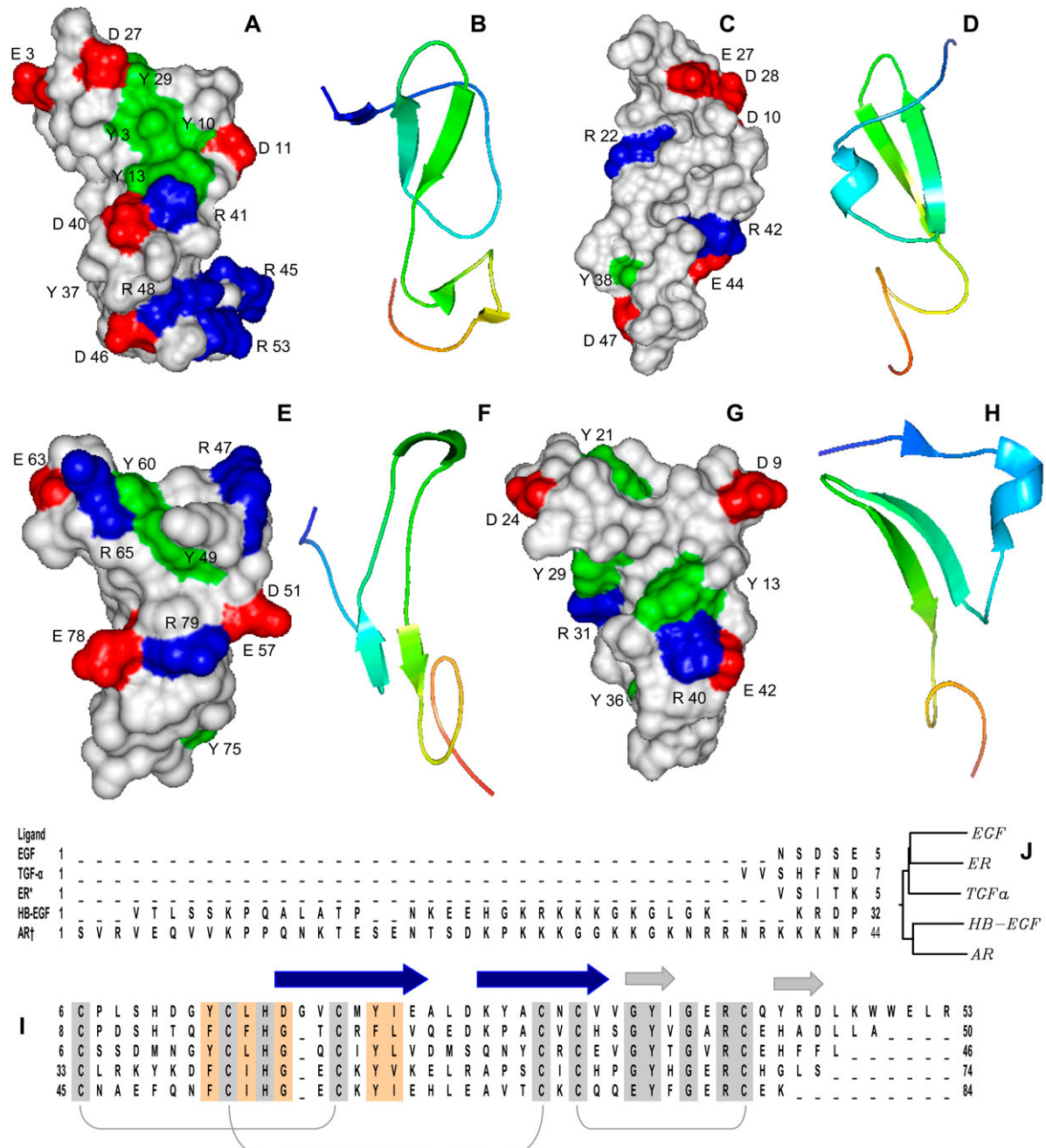
FIGURE 1 Solid surface Connolly models were generated for these ligands using their corresponding PDBs. (A) EGF (PDB:1EPJ), (C) TGF-α (PDB:1YUG), (E) HB-EGF (modified from PDB:1XDT, HB-EGF peptide composed of 79 residues), and (G) epiregulin (PDB:1K37, ER peptide composed of 46 residues). In white are the hydrophobic regions of the ligand with IR active side chains: red, negatively charged (aspartates and glutamates); blue, positive charged (arginine); and green for the tyrosine side chains. (A) The Kabash and Sander (34) rendition of these ligands is also shown to highlight the secondary structure differences (B) EGF, (D) TGF-α, (F) HB-EGF, and (H) ER, although they all contain the EGF-like domain with the characteristic two β-strands and three loops. In blue are the amino and in red are the carboxy terminal ends. (I) Sequence alignment: based on National Center for Biotechnology Information database sequences corresponding to accession numbers AAS83395, NP_003227, BAA22146 or 1K37, NP_001936, AAA51773, for human EGF, TGF-α, ER, HB-EGF, and AR, respectively.

oncogenesis. Internalization of EGFR upon binding to TGF-α occurs regularly. Furthermore, EGFR binding to TGF-α has been associated with decreased ubiquitination and an earlier dissociation of TGF-α from the receptor, as compared to EGF, in the endosomal system, under low pH conditions, resulting in enhanced recycling of EGFR (19). To date, the pharmacological profiles of these ligands during their interaction with the ErbB family of receptors remains unclear

(20). This small 50 amino acid peptide shares 45% sequence identity to EGF (21) with similar secondary structure based on the NMR and x-ray studies containing three disulfide bridges, common in this family of growth factors (12,22–33).

Several models for these ligands using the corresponding Protein Data Bank (PDB)s were generated (Fig. 1, A–H). The first is a surface Connolly representation showing the charge distribution (specifically glutamate, aspartate, and arginine) and tyrosine residues, which can be monitored via FT-IR spectroscopy for EGF, TGF-α, HB-EGF, and ER (Fig. 1, A, C, E, and G), respectively (21,26,27,30,31). Second is the Kabash and Sander representation (34), which highlights the structural motifs for four of the five ligands, with their respective loops, varying length antiparallel β-sheets, short helical motif, and random coil contributions for EGF, TGF-α, HB-EGF, and ER (Fig. 1, B, D, F, and H), respectively. The sequence comparison and dendogram (Fig. 1, I and J) is summarized based on shared identity with EGF as 45%, 40%, 41%, and 43% for TGF-α, HB-EGF, ER, and AR, respectively. EGF and TGF-α have been further studied by disulfide scrambling (35), site-directed mutagenesis (36,37), generation of chimeras (38), circular dichroism (39), and NMR (12,30,31).

H/D exchange experiments using attenuated total reflection (ATR) (40–44) FT-IR spectroscopy (45) has been used routinely to study proteins. The advantage of this study is that H→D exchange does not perturb the protein's secondary structure (46,47). The amide I band in infrared spectroscopy is very sensitive to backbone conformation and is able to distinguish several structural motifs (48–52). Typically, spectral band intensity changes are observed for the amide II (1500–600 cm^{-1}) and amide II′ (1400–1500 cm^{-1}) bands upon exposure of the protein to D_2O vapor. The concomitant band intensity changes are indicative of H→D exchange. In addition to amide vibrational modes, which provide secondary structure information, the arginine and the tyrosine side-chain modes (53–55) have exchangeable protons that can provide information on the extent of solvation in their immediate surroundings, thus acting as an internal probe. The spectral data analysis was performed using 2DCOS to enhance spectral resolution and determine the order of events during the H/D exchange process (41,42,56–58) for each ligand.

We report the results for the H/D exchange studies for EGF, TGF-α, HB-EGF, AR, and ER, which are five of the eight known ligands for the EGFR within the ErbB family of tyrosine kinase receptors. These studies will be used for future comparison with the receptor-ligand complexes. The results summarized in this article, to our knowledge, provide the first secondary structure information for AR and HB-EGF in their unbound state. Also, we compared the available
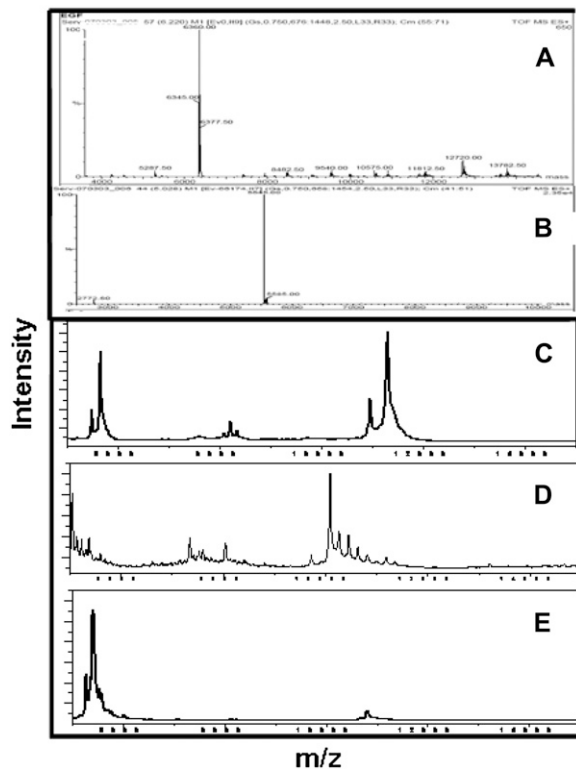
FIGURE 2 MS analysis: TOF-ES MS spectra of (A) EGF, (B) TGF-α and MALDI, (C) AR, (D) HB-EGF, and (E) ER. EGF and HB-EGF are in dimer states, whereas TGF-α, AR, and ER are in their monomeric state.

FIGURE 3 Overlaid spectra of EGFR ligands corresponding to initial and final spectra collected during the H/D exchange experiment within the spectral region of 3600–1400 cm^{-1} for (A) EGF, (B) TGF-α, (C) AR, (D) HB-EGF, and (E) ER. The spectra demonstrate the extent of hydration of the protein film and the overall band shifts and intensity changes for all five ligands.

TABLE 1 Summary of the kinetics of exchange for five of the EGFR ligands: EGF, TGF-α, AR, HB-EGF, and ER

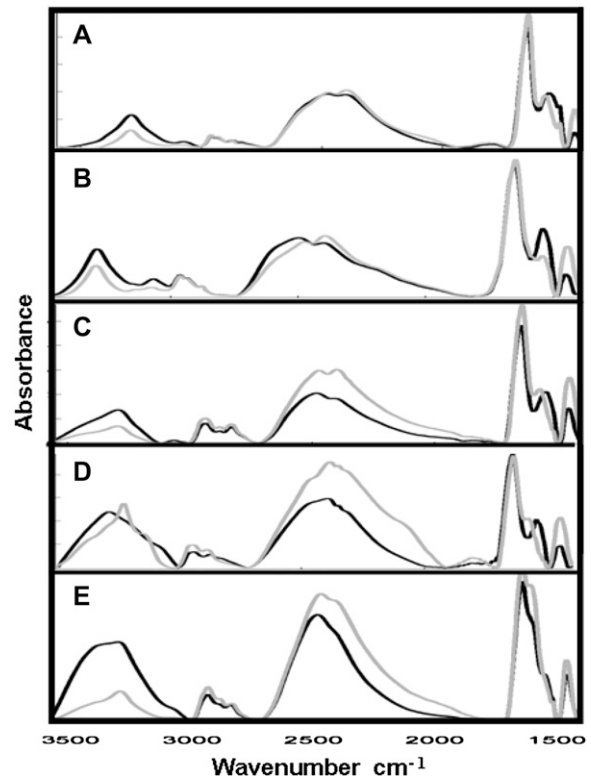| EGFR ligand	Oligomeric state	Percent secondary structure				Method	Extent of exchange	Tyr min^{-1}	Arg min^{-1}	β-turn min^{-1}	β-sheets min^{-1}	3_{10}-helix min^{-1}
		3_{10}	β	β-turn	rc							
EGF	monomer/dimer	—	26.4	11.3	62.3	NMR	40%	0.20	0.09	0.09	1.88×10^{-3}	1.88×10^{-3}
		2.9	28.5	4.7	63.8	IR						
TGF-α	monomer	6.0	20.0	8.0	66.0	NMR	65%	0.91	0.27	0.27	1.41×10^{-4}	1.41×10^{-4}
		6.3	18.8	17.8	57.1	IR						
AR	monomer	—	—	—	—	None	55%	0.47	0.04	1.00×10^{-4}	1.00×10^{-4}	1.00×10^{-4}
		2.5	25.2	6.3	66.0	IR						
HB-EGF	monomer/dimer	3.8	7.6	5.1	83.5	x-ray	65%	0.89	0.14	1.00×10^{-3}	1.00×10^{-3}	$0.89/1.00 \times 10^{-3}$
		1.5	30.6	2.4	65.5	IR						
ER	monomer	6.5	21.7	8.0	63.8	NMR	98%	0.16	0.03	1.00×10^{-4}	1.00×10^{-4}	1.00×10^{-4}
		3.6	24.0	8.0	64.4	IR						

structural information for EGF, TGF-α, HB-EGF, and ER with the FT-IR curve fitting analysis for percent secondary structure determination. In addition, a comparative analysis of the ligands' H/D exchange kinetics and their extent of exchange along with their oligomeric state via mass spectral analysis are presented. Furthermore, the H/D exchange kinetics was only one aspect of the analysis since 2DCOS analysis was also carried out and proven useful to determine the differences in the exchange process of these ligands. These results are essential to understanding the solvation properties and their oligomeric state when unbound to their receptor.

MATERIALS AND METHODS

Commercially pure (~97%) recombinant human EGF (6.3 kDa) and TGF-α (6 kDa) expressed from *Escherichia coli* were purchased from Sigma-Aldrich (St. Louis, MO) and lyophilized to remove residual acetonitrile and trifluoroacetic acid. These ligands were then resuspended in 10 mM HEPES, 100 mM NaCl buffer at pH 7.4. The other three human recombinant ligands were of high purity (~97%) and purchased from R&D Systems (Minneapolis, MN). AR (11 kDa) and ER (5.4 kDa) were also expressed from *E. coli*, and HB-EGF (9.5 kDa) was expressed from *Sf*21 insect cell cultures using a baculovirus expression system. These three ligands were not subjected to further purification. Each ligand was dialyzed against 10 mM HEPES, 100 mM NaCl at pH 7.4. All other reagents purchased were of the highest quality commercially available. All the protein samples had a final concentration of ~1 mg/mL.

The solubilized ligand was then spread onto a ZnSe ATR crystal from Thermo Electron (Madison, WI) to obtain a uniform protein film. The sample was dried overnight with a flow of dry air. Spectral acquisition was done using a Mattson Infinity Series FT-IR spectrophotometer equipped with a mercury cadmium telluride detector (Thermo Electron) under continuous dry air purge conditions. Typically, 64 scans were coadded and apodized with a triangular function to yield a resolution of 2 cm^{-1}. Before H/D exchange, a time 0 spectrum was acquired; this spectrum is characteristic of the un-exchanged ligand. For EGF, spectra were acquired every 41 s for ~5 h of the experiment, for a total of 129 spectra collected. For TGF-α, subsequent spectra were acquired every minute for the first 20 min of the exchange followed by every 15 min. In the case of EGF and TGF-α, longer spectral acquisitions were also carried out without change in the longer timeframes. For both AR and ER, subsequent spectra were acquired every 45 s the first 10 min and every 10 min after that for 7 h. For HB-EGF, spectra were acquired every 45 s the first 10 min and every 10 min after that for 14 h of the experiment to monitor the exchange. Finally, a spectrum was collected that was characteristic of the fully deuterated ligand 24 h after the first spectrum was acquired.

Spectral data analysis

No data were manipulated except for baseline correction. As a separate analysis, Fourier self-deconvolution was performed to determine the existence of minor contributing peaks. The deconvolution parameters used for
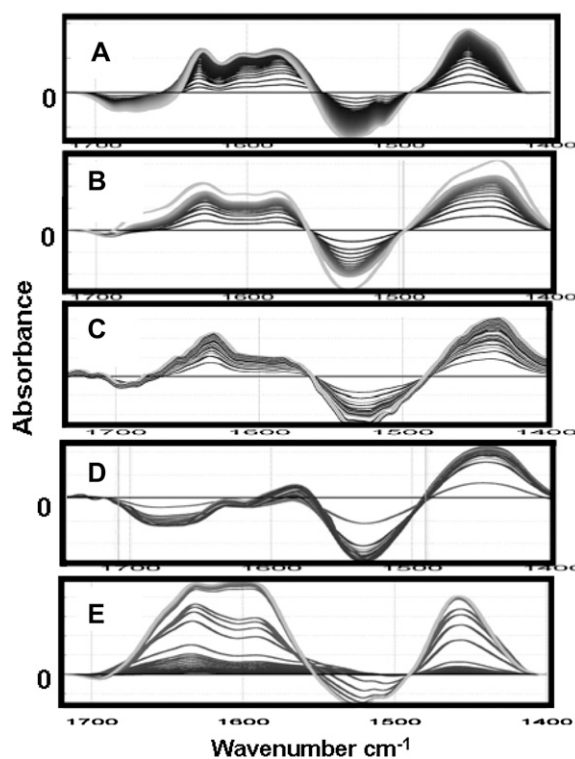

FIGURE 4 Overlaid difference spectra of the EGFR ligands. (*A*) EGF, (*B*) TGF-α, (*C*) AR, (*D*) HB- EGF, and (*E*) ER within the spectral region 1725–1400 cm^{-1}. The difference spectra were generated by subtraction of the first spectrum from all subsequent spectra.

this analysis were full width at half height of 18 cm^{-1}, and a resolution (k) was set as 2.

Assuming individual exchangeable protons, including amide protons and side-chain exchangeable protons, behave as first order kinetics,

$$H(t) = \sum_{i=1}^{N} \exp(-k_i t), \qquad (1)$$

where N is the number of amino acids, H is hydrogen, k_i is the individual rate constant for each proton, and t is time.

In a protein, these exchangeable protons are treated by class of amide group (3_{10}-helix, β-sheets, β-turns or loops, as per assignments) or exchangeable protons within side chains that are infrared (IR) active (Arg and Tyr, as per assignments). The intensity for each conformational subband and side-chain contribution within the amide I and II bands are plotted as a function of time and termed "single frequency kinetics". These data are then used to determine a multiexponential decay of the amide I and II bands upon exchange:

$$H(t) = \sum_{J=1}^{M} A_j \exp(-k_j t), \qquad (2)$$

where M is the number of protons within a class, A_j is the class of proton, and k_j is the rate constant for the class of protons.

The single frequency kinetics versus time and the $H(t)$ versus time plots are used to define and assign the slow, intermediate, and fast kinetics of exchange. The kinetics program for MATLAB (MathWorks, Natick, MA) was developed and generously provided by Dr. Erik Goormaghtigh from the Free University of Brussels, Belgium, for spectral analysis.

RESULTS AND DISCUSSION

Although these ligands were of commercial origin, time of flight (TOF) matrix assisted laser desorption ionization (MALDI)-electrospray (ES) + MS for EGF and TGF-α and MALDI MS analyses were carried out for AR, HB-EGF, and ER to verify purity, oligomeric state, and molecular weight of each ligand sample (Fig. 2). For EGF (Fig. 2 A), a peak corresponding to the monomer form at 6,360.0 mass/charge ratio (m/z) along with a dimer at 12,720.0 m/z of this ligand is commonly observed for the recombinant form of this protein. In the case of TGF-α (Fig. 2 B), a prominent peak at 5,545.0 m/z along with a minor peak at 2,772.0 m/z for the double protonated species agreed well with the calculated molecular weight of TGF-α. For AR (Fig. 2 C), a major peak observed at 11,297.0 m/z agrees well with the expected molecular weight and a shoulder at 10,956.0 m/z, which would account for the loss of the first three amino acids in the sequence (Ser, Val, and Arg). A second peak was observed at 5,651.4 m/z and a shoulder at 5,481.4 m/z, which would account for the double protonated species. A third peak is observed for AR at 8,206.0 m/z with two minor shoulders at 8,333.6 m/z and 8,078.7 m/z of the single protonated species, possibly due to proteolytic cleavage from the Lys-N protease (based on results obtain from the Expasy peptide cutter subroutine

FIGURE 5 The kinetics of exchange for EGF is summarized in three plots. (A) Initial times of exchange. (B) Percent of unexchanged protein versus time. EGF was observed to exchange 40% after 80 min. A straight line shown at the bottom of each multiexponential decay plot (A and B) is the residual of the fit with the resulting standard deviation 0.039. (C) Evolution of the absorbance at selected wavenumbers versus time, which includes a summary of the kinetic components assigned to Tyr, Arg, and the different structural motifs.

cm^{-1}	Sub-band	Rate (min^{-1})
1580	Arg	0.09
1690	β-turn	0.09
1600	Arg	0.09
1630/1647	β-sheet/3_{10}-helix	1.88 x10^{-3}
1545	NH-deformation	0.20
1520	Tyr	0.20

(59))—in this case, accounting for the loss of the first 25 residues within the sequence and consequently the loss of the random coil portion found at the N-terminal end of this ligand, thus allowing the conformational analysis AR.

For HB-EGF (Fig. 2 *D*), the parent peak at 9,721.3 m/z, a second peak at 10,088 m/z with a series of shoulders at 10,263, 10,453, 10,629, 10,813, 10,995, 11,184, and 11,358 m/z are due to heterogeneous O-glycosylation. Third and fourth peaks, observed for HB-EGF at 8,040.7 m/z with shoulders at 7,601.3, 7,529.7, and 7,345.5 m/z are possibly due to proteolysis. Specifically, the peak at 8,040.7 m/z would be due to a proteolytic cleavage of the first four residues including Ser_4 in the O-glycosylated state, followed by 7,601.3 m/z due to an additional loss of four residues (Ser_5–Gln_8), whereas 7,529.7 and 7,345.5 m/z are due to the further loss of one to three residues (Ala_9 and Leu_{10}-Ala_{11}), respectively. A fifth peak at 5,047.3, with shoulders at 5,135.2, 5,230.0, 5316.1, 5,374.4, and 5,595.4 m/z, are the double protonated species of HB-EGF O-glycosylated ligand. For ER (Fig. 2 *E*) the MALDI showed two peaks, a major peak was observed at 5,401.8 m/z with three shoulders at 5,270.0,

5,547.5, and 5,585.9 m/z corresponding to the single protonated species along with nonspecific proteolytic cleavage products of ER, respectively. The second minor peak, observed at 10,815 m/z, was assigned to the dimer form of ER. Assuming monomer and dimer forms ionize at the same rate, the dimer contribution for ER is small. The MS analysis of these ligands corresponds to the calculated protein masses (EGF, TGF-α, AR, and ER), their proteolytic cleavage products (AR, HB-EGF, and ER), their posttranslational modification (HB-EGF), and their dimer forms (EGF and ER). Otherwise, these ligands were pure protein products.

FT-IR spectroscopy

Typical ATR-FT-IR spectra for a D_2O hydrated uniform protein film in the spectral region of 3600–1400 cm^{-1} for EGF, TGF-α, AR, HB-EGF, and ER (Fig. 3, *A–E*, respectively) are composed of the amide A band ($\sim$3200 cm^{-1}), the amide I′ band ($\sim$1650 cm^{-1}), the amide II band ($\sim$1540 cm^{-1}), and the amide II′ band ($\sim$1450 cm^{-1}). We closely monitored the spectral changes in the spectral region 1700–
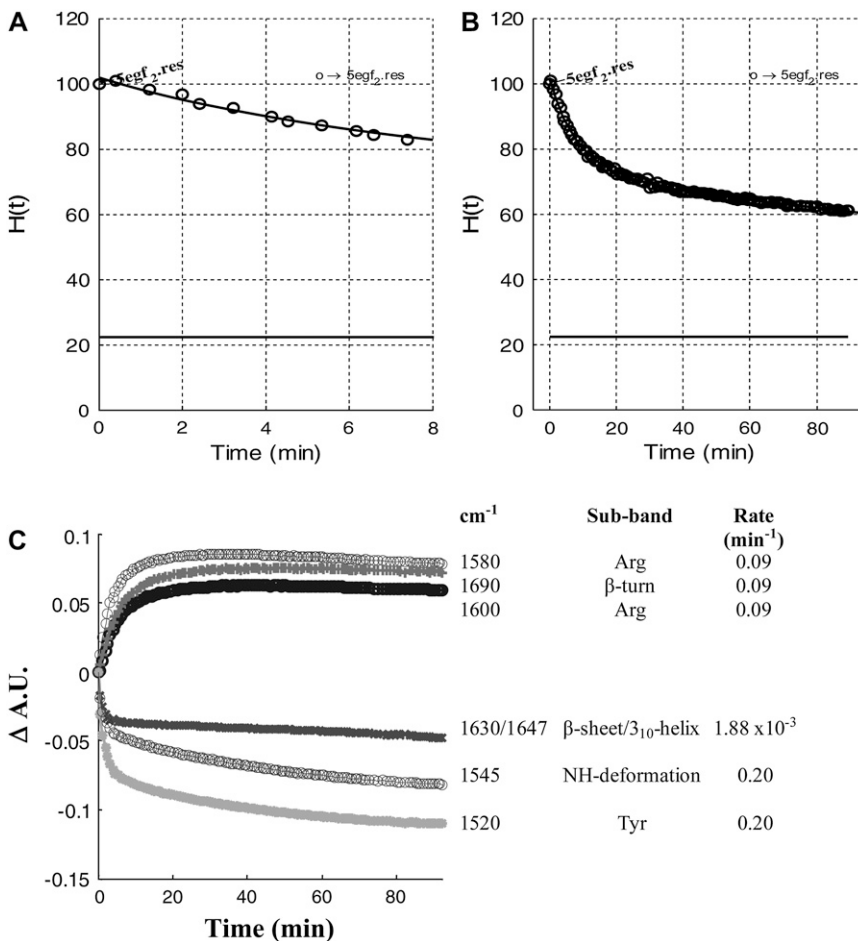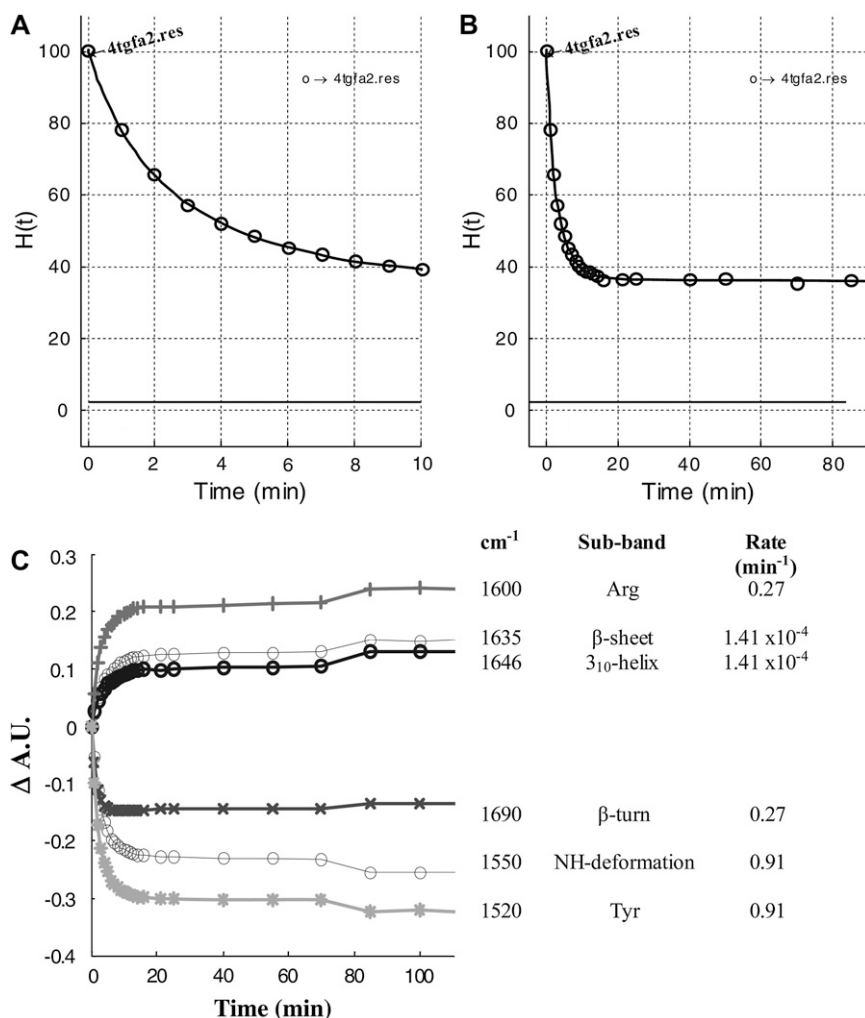

FIGURE 6 The kinetics of H/D exchange for TGF-α is summarized in three plots. (*A*) Initial times of exchange. (*B*) Percent of unexchanged protein versus time. TGF-α was observed to exchange 65% after 15 min. A straight line shown at the bottom of each multiexponential decay plot (*A* and *B*) is the residual of the fit with the resulting standard deviation 0.071. (*C*) Evolution of the absorbance at selected wavenumbers versus time, which includes the kinetics assigned for Tyr, Arg, and the different structural motifs.

cm^{-1}	Sub-band	Rate (min^{-1})
1600	Arg	0.27
1635	β-sheet	1.41×10^{-4}
1646	3_{10}-helix	1.41×10^{-4}
1690	β-turn	0.27
1550	NH-deformation	0.91
1520	Tyr	0.91

1400 cm^{-1} during H→D exchange to include the observed shift of the amide I′ band form accompanied by an increase in bandwidth. In addition, a decrease in intensity of the amide II band at ∼1540 cm^{-1} along with a concomitant increase of the amide II′ band at ∼1450 cm^{-1} were observed. These spectral changes were studied in detail by curve fitting analysis, difference spectroscopy, 2DCOS analysis, and H/D exchange kinetics.

Curve-fitting analysis (spectral data not shown) was performed for the determination of percent secondary structure for each ligand, as summarized in Table 1. Except for AR, these results were compared with the available high-resolution structural data. For EGF the percent secondary structure contributions were 2.9% 3_{10}-helix, 28.5% β-sheet, 4.7% β-turn, and 63.8% random coil. The EGF results for the β-sheet and random coil contributions are in good agreement with NMR results (PDB:1EPJ) (20–25) at pH 6.6, although our experimental conditions were different, and the pH 7.4 and the presence of dimer species may account for the small contribution of 3_{10} helix and the lower 4.7% β-turn contribution—as for TGF-α, 6.3% 3_{10}-helix, 18.8% β-sheet, 17.8% β-turn, and 57.1% random coil contribution. The TGF-α results for

the 3_{10}-helix and β-sheet contribution are in good agreement with NMR results (PDB:1YUG) (25,31,32). Furthermore, the first structural analysis for AR resulted in 2.5% 3_{10}-helix, 25.2% β-sheet, 6.3% β-turn, and 66.0% random coil contribution.

HB-EGF is composed of 1.5% 3_{10}-helix, 30.6% β-sheet, 2.4% β-turn, and 65.5% random coil contribution. This result accounts for the only available percent secondary structure for the HB-EGF in its unbound state. However, the results presented above for HB-EGF are not in agreement with the bound ligand in complex with diphtheria toxin (PDB:1XDT) (11), suggesting that the ligand changes its secondary structure when bound. A second important factor for the disagreement is that the x-ray structure of recombinant diphtheria toxin/HB-EGF complex was obtained using *E. coli* as host; so, HB-EGF in this structure is not glycosylated, whereas our results are for *Sf*21 host recombinant HB-EGF in the O-glycosylated state, potentially also accounting for the different secondary structure contributions. Finally, ER's secondary structure is composed of 3.6% 3_{10}-helix, 24.0% β-sheet, 8.0% β-turn, and 64.4% random coil contribution, which is in reasonably good agreement with the available NMR structural information (PDB:1K37) (14).
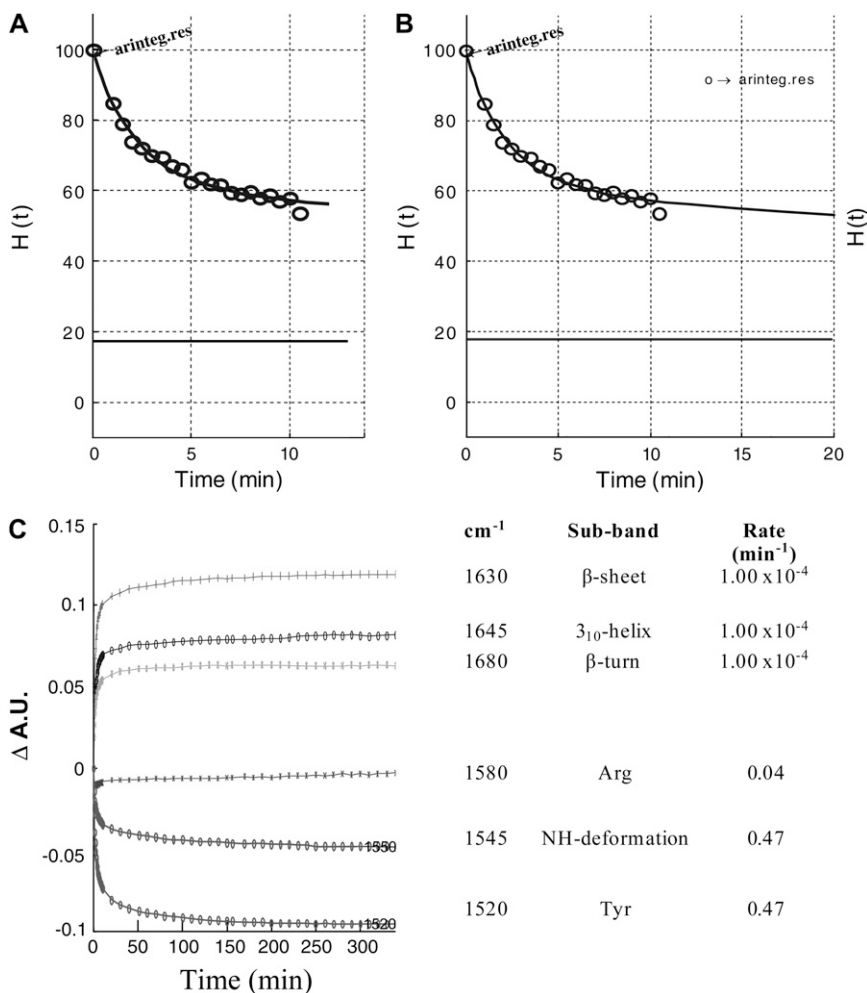

FIGURE 7 The kinetics of exchange for AR is summarized in three plots. (*A*) Initial times of exchange. (*B*) Percent of unexchanged protein versus time. AR was observed to exchange 55% after 80 min. A straight line shown at the bottom of each multiexponential decay plot (*A* and *B*) is the residual of the fit with the resulting standard deviation 0.083. (*C*) Evolution of the absorbance at selected wavenumbers versus time, which includes a summary of the kinetic components assigned to Tyr, Arg, and the different structural motifs.

cm^{-1}	Sub-band	Rate (min^{-1})
1630	β-sheet	1.00×10^{-4}
1645	3_{10}-helix	1.00×10^{-4}
1680	β-turn	1.00×10^{-4}
1580	Arg	0.04
1545	NH-deformation	0.47
1520	Tyr	0.47

The difference spectra were obtained by subtracting the first spectrum from all subsequent spectra for the spectral region of 1720–1400 cm^{-1}. A summary of the peak assignment for the maxima (+) or minima (−) resulting from the increase or decrease in overall peak intensities is listed below. For EGF, the peak assignments are composed of β-turn ((−) 1690 and 1680 cm^{-1}), random coil ((+) 1659 cm^{-1}), strong β-sheet contribution ((+) 1630 cm^{-1}), Arg side-chain modes ((+) 1600 cm^{-1} and 1580 cm^{-1}), N-H deformation mode ((−) 1545 cm^{-1}), Tyr side-chain mode ((−) 1520 cm^{-1}), and N-D deformation mode ((+) 1450 cm^{-1}) as shown in Fig. 4 A. For the resulting difference spectra for TGF-α difference spectra, the peak assignments are composed of β-turn ((−) 1690 cm^{-1}), random coil ((+) 1673 cm^{-1}), 3$_{10}$-helix ((+) 1646 cm^{-1}), β-sheet ((+) 1635 cm^{-1}), Arg side-chain modes ((+) 1600 cm^{-1}), N-H deformation mode ((−) 1550 cm^{-1}), Tyr side-chain mode ((−) 1520 cm^{-1}), and N-D deformation mode ((+) 1450 cm^{-1}), as shown in Fig. 4 B.

The difference spectra for AR are composed of β-turn ((−) 1685 and 1680 cm^{-1}), random coil ((+) 1660 cm^{-1}), 3$_{10}$-helix ((+) 1645 cm^{-1}), strong β-sheet contribution ((+) 1630 cm^{-1}), Arg side-chain modes ((+) 1580 cm^{-1}), N-H defor-

mation mode ((−) 1545 cm^{-1}), Tyr side-chain mode ((−) 1520 cm^{-1}), and N-D deformation mode ((+) 1450 cm^{-1}), as shown in Fig. 4 C. The difference spectra for HB-EGF are composed of β-turn ((−) 1675 cm^{-1}), random coil ((+) 1655 cm^{-1}), 3$_{10}$-helix ((+) 1650 cm^{-1}), strong β-sheet contribution ((+) 1630 cm^{-1}), Arg side-chain modes ((+) 1582 cm^{-1}), N-H deformation mode ((−) 1550 cm^{-1}), Tyr side-chain mode ((−) 1520 cm^{-1}), and N-D deformation mode ((+) 1450 cm^{-1}), as shown in Fig. 4 D. The difference spectra for ER are composed of β-turn ((−) 1675cm^{-1}), random coil ((+) 1655 cm^{-1}), 3$_{10}$-helix ((+) 1645 cm^{-1}), strong β-sheet contribution ((+) 1630 cm^{-1}), Arg side-chain modes ((+) 1600 cm^{-1}), N-H deformation mode ((−) 1545 cm^{-1}), Tyr side-chain mode ((−) 1520 cm^{-1}), and N-D deformation mode ((+) 1445 cm^{-1}), as shown in Fig. 4 E.

Kinetics of exchange

The kinetics of H/D exchange were carried out for these five ligands using no prior knowledge of the constants, but rather doing a systematic assessment of the intensities every 10 wavenumbers for the amide II band with time. For purposes
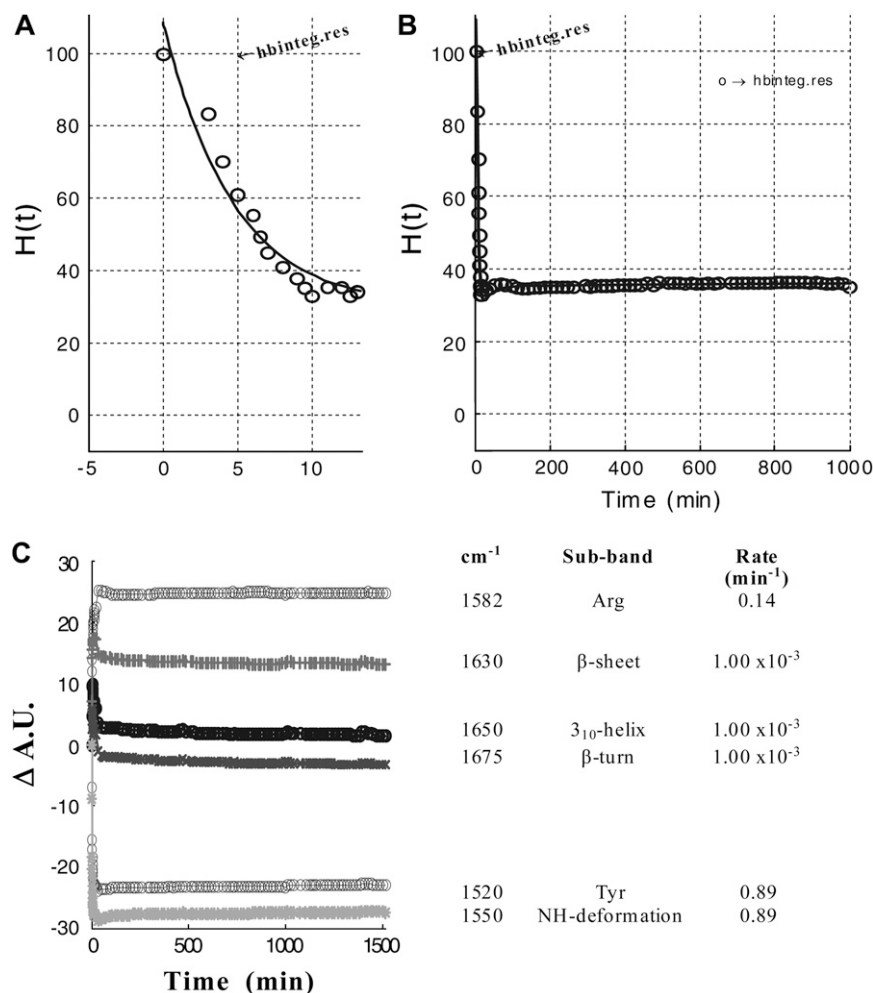

FIGURE 8 The kinetics of exchange for HB-EGF is summarized in three plots. (A) initial times of exchange. (B) Percent of unexchanged protein versus time. HB-EGF was observed to exchange 65% after 20 min. A straight line shown at the bottom of each multiexponential decay plot (A and B) is the residual of the fit with the resulting standard deviation 0.127. (C) Evolution of the absorbance at selected wavenumbers versus time, which includes a summary of the kinetic components assigned to Tyr, Arg, and the different structural motifs.

cm^{-1}	Sub-band	Rate (min^{-1})
1582	Arg	0.14
1630	β-sheet	1.00 x10^{-3}
1650	3$_{10}$-helix	1.00 x10^{-3}
1675	β-turn	1.00 x10^{-3}
1520	Tyr	0.89
1550	NH-deformation	0.89

FIGURE 9 The kinetics of exchange for ER is summarized in three plots. (*A*) Initial times of exchange. (*B*) Percent of unexchanged protein versus time. ER was observed to exchange 98% after 150 min. A straight line shown at the bottom of each multiexponential decay plot (*A* and *B*) is the residual of the fit with the resulting standard deviation 0.650. (*C*) Evolution of the absorbance at selected wavenumbers versus time, which includes a summary of the kinetic components assigned to Tyr, Arg, and the different structural motifs.
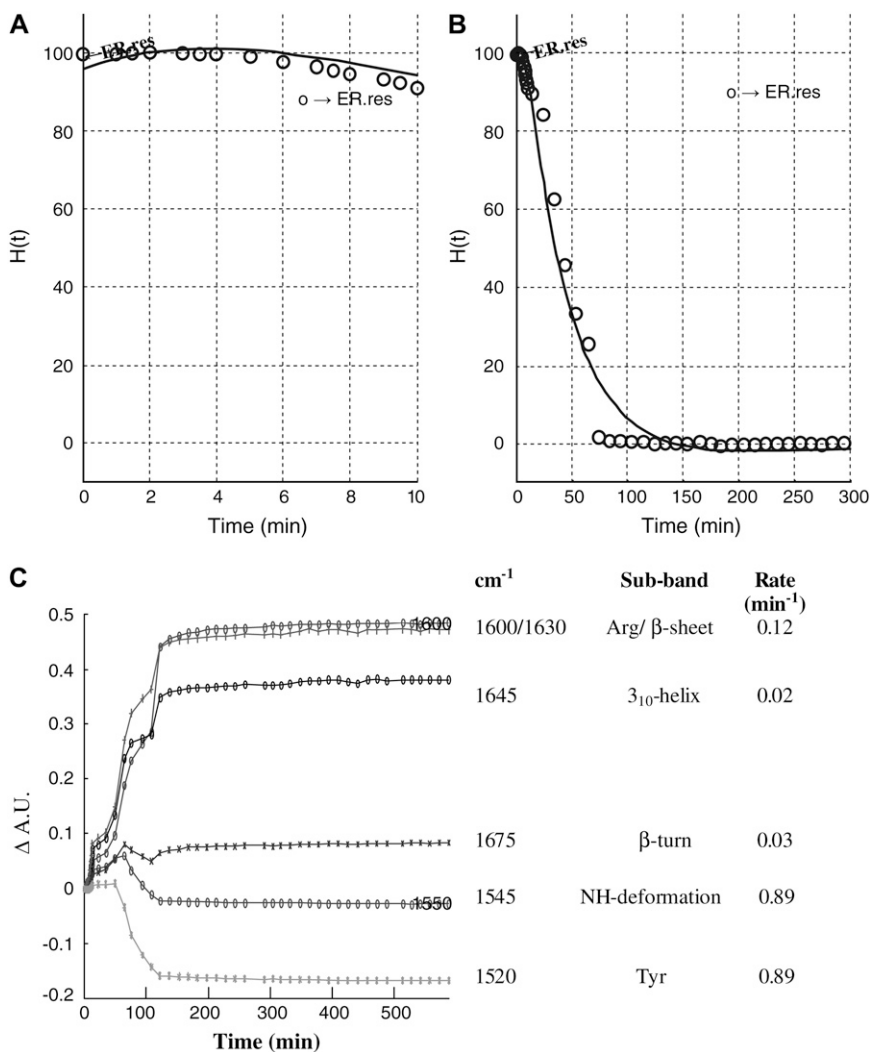
of clarity, only the intensities associated with known assignments were plotted as the evolution of the absorbance at selected wavenumber versus time. The intensity at ~1550 cm^{-1} was normalized using the intensity of the isobestic point of the amide I' band to generate a plot of the percent of unexchanged protein versus time. The amide I band isobestic points were 1673, 1687, 1673, 1671, and 1695 cm^{-1} for EGF, TGF-α, AR, HB-EGF, and ER, respectively. The difference in isobestic point could be due to the different contributions of small 3_{10}-helical domains and β-turns.

The overall extent of exchange for each ligand is shown in Figs. 5, *A* and *B*, to 9, *A* and *B*, and is summarized in Table 1. In general, the extent of exchange agreed with the overall hydrophobic residue content for each ligand (as analyzed by the Kyte-Doolittle hydropathy sequence analysis (60)), oligomeric state, and glycosylation. The exception was AR, suggesting that the polar residues may be buried, whereas the hydrophobic residues mainly located within C-terminal end are exposed. The fastest initial exchange was observed for TGF-α: within the first 5 min of the exchange process, 50%

of the ligand had exchanged. The next fastest initial exchange was HB-EGF: within the first 5 min, 40% had exchanged, probably due to the glycosylation. Although ER had the slowest initial exchange, it was also this ligand that underwent complete exchange, suggesting that the dimer species is present in small quantities and that this protein is almost completely exposed to its aqueous environment. The extent of H/D exchange for these ligands, with EGF having the lowest extent of exchange, suggests the dimer form contributed to the loss of exposure to its aqueous environment with only 40%; in contrast, epiregulin had almost complete exchange (98%). HB-EGF had a greater extent of exchange, i.e., 65%, suggesting the glycosylation affected hydration of the ligand, whereas TGF-α and AR had extents of exchange of 65% and 55%, respectively.

The kinetics of exchange can be used to study the dynamic factors that affect hydrogen-bonding interactions which are dependent on the secondary structure of the protein, in the case of the amide protons, and the local environment observed for the side chains, thus affecting protein stability.

These results were determined for several secondary structural motifs—arginine and tyrosine residues (Figs. 5 *C* to 9 *C*)—and summarized in Table 1. HB-EGF and TGF-α have the same exchange rates for Tyr, suggesting these residues are in similar environments. Also for AR, HB-EGF, and ER, the rates for Arg and Tyr were faster than the backbone exchange rates. HB-EGF had two different exchange rates for the 3_{10}-helices, suggesting two different environments. EGF and HB-EGF had similar exchange rates for the β-sheets, whereas TGF-α, ER, and AR were 10 orders of magnitude slower. Finally, for AR the secondary structure motifs had the same exchange rate in this case; the order of events ascertained from 2DCOS proved valuable because it helped establish the differences in H/D exchange for these domains. In general, the order of events ascertained from the 2DCOS agreed with the kinetic analysis, with few exceptions, due to the extremely fast exchange process of certain components, such as exposed Tyr and the random coils.

2D-COS

To enhance the spectral resolution and extract correlation and temporal information of the spectral changes, a two-dimensional correlation analysis was performed on each data set, within the spectral region of 1800–1400 cm^{-1}. The synchronous plots, which reflect in-phase transitions, are shown in Figs. 10, *A* and *C*, and 11, *A*, *C*, and *E*; and the asynchronous plots, which reflect out-of-phase transitions, are shown in Figs. 10, *B* and *D*, and 11, *B*, *D*, and *F*, for EGF, TGF-α, AR, HB-EGF, and ER, respectively. The auto peaks are diagonal peaks, which reflect intensity variations, whereas crosspeaks are off-diagonal peaks, reflecting correlations. These assignments are summarized in Table 2. At times, there can be small contributions that are difficult to localize due to band overlapping. To confirm the presence of small overlapped peaks, the spectral data were deconvolved (data not shown).

Synchronous plots

Several differences in the peak pattern between the three ligands (EGF, TGF-α, AR, HB-EGF, and ER) are observed. The synchronous plots are shown in Fig. 10, *A* and *C*, for EGF and TGF-α and in Fig. 11, *A*, *C*, and *E*, for AR, HB-EGF and ER, respectively. The auto peak and crosspeak assignments are summarized in Table 2. The largest intensity changes for the auto peaks were the N-H and N-D deformation modes ($\sim$1550 cm^{-1} and $\sim$1450 cm^{-1}, respectively) associated primarily with backbone amides. In general, the backbone and side-chain (Arg, Tyr) vibrational modes correlated with the N-H
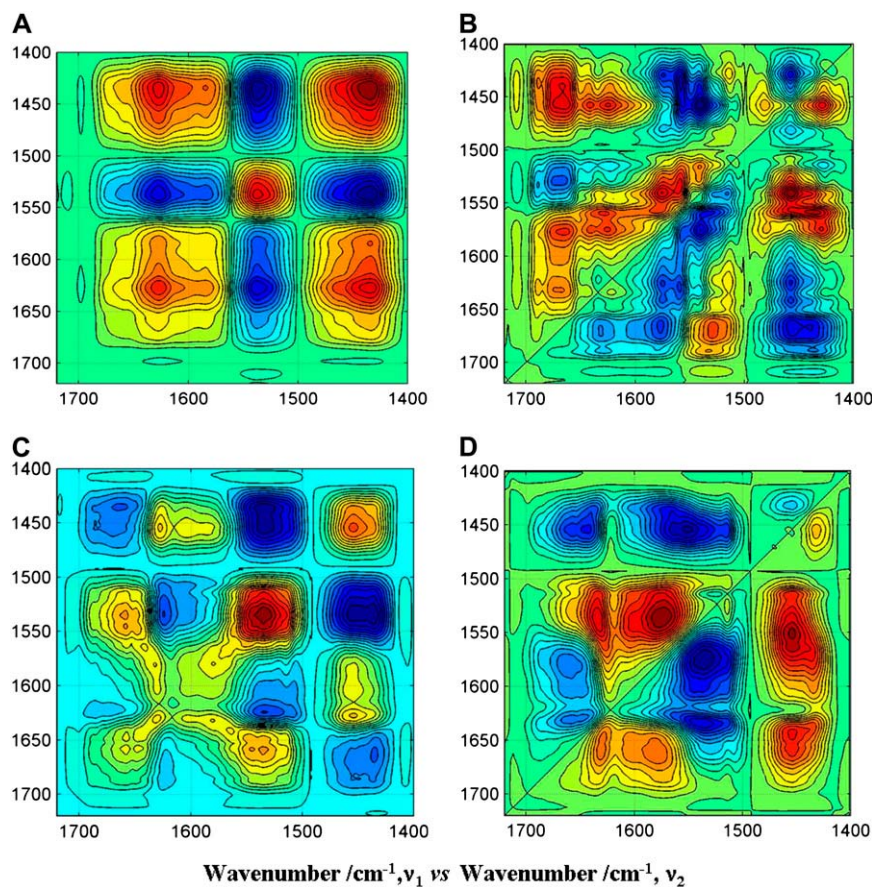

FIGURE 10 2DCOS obtained from the baseline-corrected spectra corresponding to EGF and TGF-α (*A* and *C*) synchronous and (*B* and *D*) asynchronous plots, respectively.
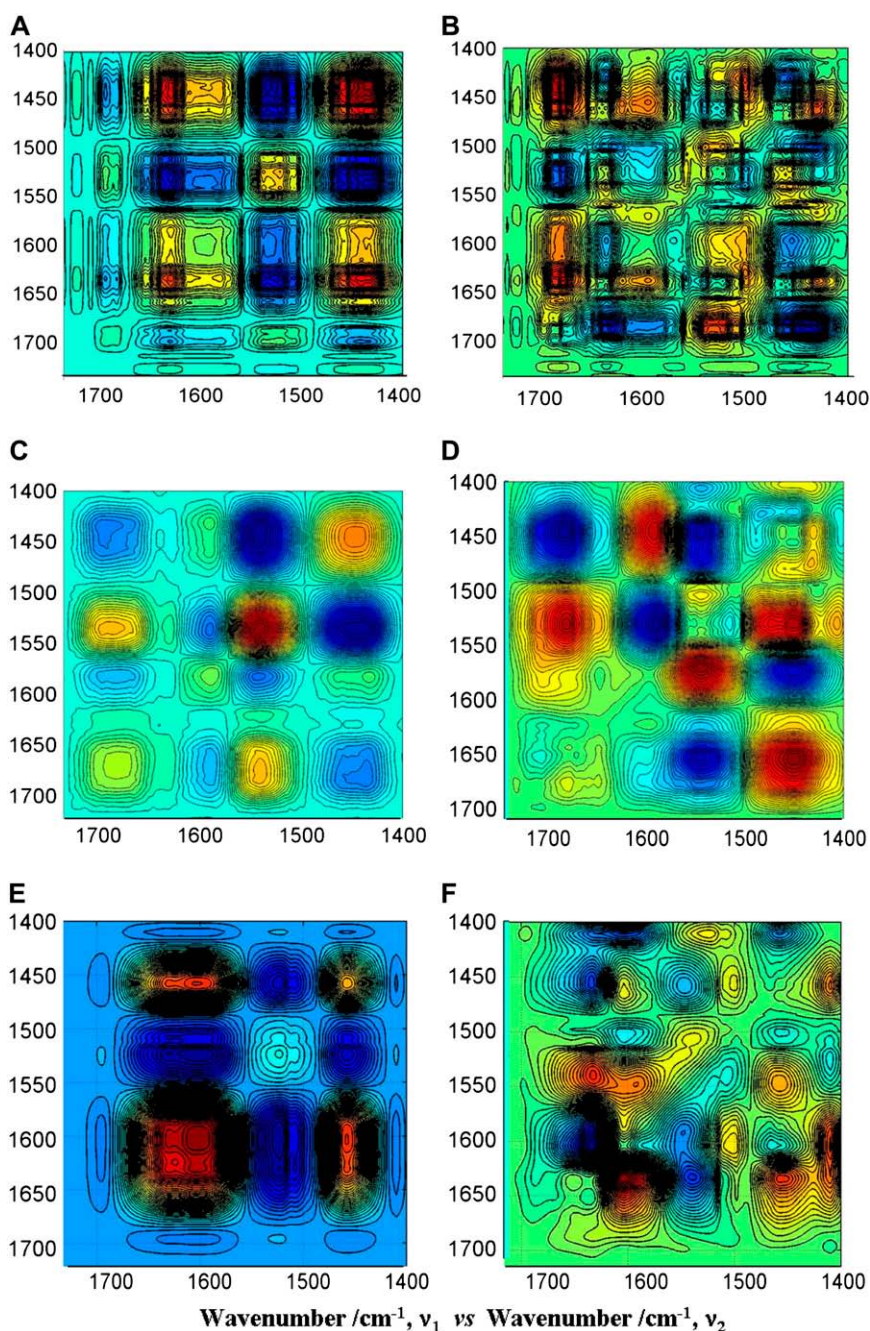
Wavenumber /cm^{-1},ν_1 *vs* Wavenumber /cm^{-1}, ν_2

FIGURE 11 2DCOS corresponding to AR, HB-EGF, and ER obtained from the baseline corrected spectra (*A*, *C*, and *E*) synchronous plots and (*B*, *D*, and *F*) asynchronous plots, respectively.

and N-D deformation modes. The β-turns in EGF were observed to be in two different environments, suggesting that the backbone dynamics were different.

Synchronous plots for each ligand are shown in Fig. 10, *A* and *C*. For EGF the β-sheets (1630 cm^{-1}) and β-turns correlate with the Arg (1600 and 1580 cm^{-1}) and Tyr modes (1520 cm^{-1}). For TGF-α, the 3_{10}-helix (1646 cm^{-1}) correlates with Arg mode (1600 cm^{-1}), whereas the β-turns (1690 cm^{-1}) correlate with the β-sheets (1635 cm^{-1}) and Tyr (1520 cm^{-1}) vibrational mode. Of all the ligands in this study, the highest degree of complexity in the 2DCOS plots was observed for AR (Fig. 11 *A*). The similarity in these patterns will be discussed in

terms of the position of the auto peaks; and their assignments at 1680, 1685 cm^{-1} (β-turns), 1630 cm^{-1} (β-sheet), and Arg (1580 cm^{-1}) resembles those of AR (Fig. 11 *A*). The β-sheets (1630 cm^{-1}) and helical (1645 cm^{-1}) motifs govern the exchange process in AR. The β-sheets (1630 cm^{-1}) are correlated well with the Arg (1580 cm^{-1}), the Tyr (1520 cm^{-1}), and the β-turn (1680 cm^{-1}). Finally, for AR the β-turns (1685 cm^{-1}) also correlate with the Tyr mode (1520 cm^{-1}). HB-EGF (Fig. 11 *C*) resulted in its β-turns (1675 cm^{-1}) and Tyr (1520 cm^{-1}) governing the exchange process.

These peaks also correlated with each other, suggesting they are exposed to the aqueous environment. In addition,

TABLE 2 Summary of 2DCOS peak assignments for the EGFR ligands EGF, TGF-α, AR, HB-EGF, and ER synchronous autopeaks and asynchronous crosspeaks

| Assignment | EGF | | TGF-α | | AR | | HB-EGF | | ER | |
	S* autopeaks (cm^{-1})	A[†] crosspeaks (cm^{-1})	S autopeaks (cm^{-1})	A crosspeaks (cm^{-1})	S autopeaks (cm^{-1})	A crosspeaks (cm^{-1})	S autopeaks (cm^{-1})	A crosspeaks (cm^{-1})	S autopeaks (cm^{-1})	A crosspeaks (cm^{-1})
β-sheet	1630	1628	1635	1635	1630	1632	1630	1634	1630	1632
β-turn	1690, 1680	1690, 1680	1690	1690	1680, 1685	1680, 1685	1675	1680	1675	1675
3_{10}-helix	1647	1648	1646	1648	1645	1645	1650	1648	1645	1646
Arg side chain	1600, 1580	1600, 1580	1600	1600, 1585	1580	1582	1582	1582	1600	1597
N-H deformation	1545	1545	1550	1545	1545	1550	1550	1548	1545	1551
Tyr side chain	1520	1510	1520	1514	1520	1520	1520	1516	1520	1519
N-D deformation	1450	1450	1440	1450	1450	1450	1445	1451	1445	1449

*Synchronous plot.

[†]Asynchronous plot.

HB-EGF's 3_{10}-helical peak (1650 cm^{-1}) correlates with the Tyr (1520 cm^{-1}), suggesting they are also in a similar environment. Meanwhile, the exchange process in ER is governed by the Arg (1600 cm^{-1}) and β-sheets (1630 cm^{-1}), although the strongest exchange perturbation was the Arg (1600 cm^{-1}). This effect is demonstrated more strongly by the similarity in phase and position of the corresponding crosspeaks. However, for ER, there is an absence of several auto peaks—1675 cm^{-1} (β-turn) and 1645 cm^{-1} (3_{10}-helix) auto peaks (Fig. 11 E)—suggesting that these motifs are less exposed to their aqueous environment, unlike EGF, TGF-α, AR, and HB-EGF.

Asynchronous plots

TGF-α and EGF asynchronous plots are also quite different from the asynchronous plots shown for AR, HB-EGF, and ER, suggesting differences in the dynamics of exchange (Figs. 10, B and D, and 11, B, D, and F, respectively). The color of these crosspeaks and their counterparts in the synchronous plots allows the determination of the order of events summarized in Tables 3 and 4. However, for TGF-α, spectral deconvolution was also performed to enhance the resolution of asynchronous plots (data not shown). The apparent absence of the 1690 cm^{-1} crosspeak shown in Fig. 10 D, associated with the β-turns present in TGF-α, was due to small intensity changes. Otherwise, equal crosspeak intensity distributions were observed for EGF and TGF-α (Fig. 10, B and D). In the case of EGF, the side chains correlated well with each other: Arg (1580 cm^{-1}) and Tyr (1510 cm^{-1}). Also observed were the β-sheets (1628 cm^{-1}), which correlated with the β-turns (1680, 1690 cm^{-1}).

For TGF-α, the 3_{10}-helix (1648 cm^{-1}) correlates with the β-sheets (1635 cm^{-1}), whereas the Tyr (1514 cm^{-1}) crosspeak correlated well with the Arg (1600 cm^{-1}) and the β-turn (1690 cm^{-1}). The crosspeaks observed with largest intensity changes in AR, the β-sheet (1632 cm^{-1}) and 3_{10}-helix (1645 cm^{-1}) correlates with Arg (1582 cm^{-1}), whereas the β-turns (1680, 1682 cm^{-1}) correlated with the β-sheet (1632 cm^{-1})

(Fig. 11 B). Also, the β-sheet (1632 cm^{-1}) and β-turns (1680 cm^{-1}) correlate with the Tyr (1520 cm^{-1}). For HB-EGF, it is interesting to note that the β-turn (1670 cm^{-1}) correlates inversely with the Tyr (1516 cm^{-1}) and Arg (1582 cm^{-1}) crosspeaks (Fig. 11 D). ER, the Arg peak (1597 cm^{-1}), correlates with both the β-sheets (1632 cm^{-1}) and 3_{10}-helix (1646 cm^{-1}); and the 3_{10}-helix (1646 cm^{-1}) exchanges before the β-sheets (1632 cm^{-1}).

The order of events for each ligand is as follows: for EGF the Tyr residues exchange first, followed by Arg, then the β-turn, and finally β-sheets and the 3_{10}-helix motif; whereas for TGF-α it was the Tyr, followed by the Arg, then the 3_{10}-helix and β-sheets, and finally the β-turn. In the case of AR, the Tyr residues exchanged first, followed by Arg; then the β-sheets exchange is followed by the 3_{10}-helix and finally the β-turns. For HB-EGF, the order of exchange is Tyr, followed by Arg, then the β-sheets, followed by 3_{10}-helix and β-turns. For ER, the Tyr exchanges first, followed by the β-turns, then Arg, the 3_{10}-helix, and finally

TABLE 3 Order of events during the H/D exchange process for EGF and TGF-α

Event	Order of Events*
	EGF
1	Tyr (1520 cm^{-1}) before Arg (1580 cm^{-1})
2	β-turns (1680, 1690 cm^{-1}) occur before β-sheet (1628 cm^{-1})
3	Tyr (1510 cm^{-1}) before β-sheet (1628 cm^{-1})
4	β-sheet (1628 cm^{-1}) before 3_{10}-helix (1648 cm^{-1})
5	Arg (1580 cm^{-1}) before β-turns (1680, 1690 cm^{-1})
6	Tyr (1510 cm^{-1}) occur prior β-turns (1680, 1690 cm^{-1})
	TGF-α
1	Tyr (1514 cm^{-1}) before 3_{10}-helix (1648 cm^{-1})
2	Tyr (1514 cm^{-1}) before β-sheet (1635 cm^{-1})
3	3_{10}-helix (1648 cm^{-1}) before β-sheet (1635 cm^{-1})
4	Arg (1600 cm^{-1}) before 3_{10}-helix (1648 cm^{-1})
5	Tyr (1514 cm^{-1}) before Arg (1600 cm^{-1})
6	β-sheet (1635 cm^{-1}) before β-turns (1690 cm^{-1})
7	Arg (1600 cm^{-1}) occurs before β-turns (1690 cm^{-1})

*Peak assignment and crosspeak positions are used to describe each event.

TABLE 4   Order of events during the H/D exchange process for AR, HB-EGF, and ER

Event	Order of events*
	Amphiregulin
1	Tyr (1520 cm^{-1}) before Arg (1582 cm^{-1})
2	Arg (1582 cm^{-1}) before β-sheet (1632 cm^{-1})
3	β-sheet (1632 cm^{-1}) before β-turns (1680/1682 cm^{-1})
4	β-sheet (1632 cm^{-1}) before 3_{10}-helix (1645 cm^{-1})
5	3_{10}-helix (1645 cm^{-1}) before β-turns (1680/1682 cm^{-1})
	HB-EGF
1	Arg (1582 cm^{-1}) before β-sheet (1632 cm^{-1}) and β-turns (1670 cm^{-1})
2	Arg (1582 cm^{-1}) before 3_{10}-helix (1650 cm^{-1})
3	3_{10}-helix (1650 cm^{-1}) before β-turns (1670 cm^{-1})
4	β-sheet (1632 cm^{-1}) before 3_{10}-helix (1650 cm^{-1})
	Epiregulin
1	Tyr (1520 cm^{-1}) before 3_{10}-helix (1646 cm^{-1}) and β-sheet (1632 cm^{-1})
2	Tyr (1520 cm^{-1}) before Arg (1597 cm^{-1})
3	Arg (1597 cm^{-1}) before β-sheet (1632 cm^{-1})
4	3_{10}-helix (1646 cm^{-1}) before β-sheet (1632 cm^{-1})
5	β-turn (1675 cm^{-1}) before Arg (1597 cm^{-1}) and 3_{10}-helix (1646 cm^{-1})

*Peak assignment and crosspeak positions are used to describe each event.

the β-sheet. The random coil crosspeak was never observed, due to the extremely fast kinetics of exchange occurring for our experimental setup (43). Therefore, the dynamics of exchange are different for these ligands. More importantly, these results correlate well with the kinetics of exchange presented above and were used to determine when the rates of exchange were the same.

CONCLUSION

Differences in secondary structure, conformational fluctuations, and exposure of the protein to its aqueous environment are factors that affect the dynamic nature of hydrogen-bonding interactions. By correlating the amide protons found in the backbone to the side chains, we were able to explore these factors and relate them to the oligomeric state and posttranslational modification of the protein. We chose a family of ligands that interacts with the same target protein (receptor) and has similar sequence, size, and secondary structure—thus allowing a comparative analysis.

These ligands were characterized by MS analysis and FT-IR spectroscopy. MS analysis is the technique of choice to determine the integrity and oligomeric state of a protein and as such was found to be crucial to understand the differences in the extent of exchange observed. The FT-IR spectroscopic analysis presented here for these ligands is in relatively good agreement with the available structural information (12,22–24,29–32,59). We determined the secondary structure composition for AR and HB-EGF in their unbound state. These ligands share common motifs defined by three disulfide bridges that generate three loops, two-stranded antiparallel

β-sheets, and random coil regions in the amino and carboxyl termini. These structural similarities cannot explain their roles in regulating the EGFR. Differences in the extent of exchange were not due to the differences in molecular weight, but rather the residue content affecting solvent accessibility, dimerization, and/or posttranslational modification observed for HB-EGF (glycosylation).

The fastest components to exchange were the side chains (Arg or Tyr), showing that these side chains were highly exposed to their aqueous environment, whereas the β-sheets within EGF and HB-EGF were determined to be one order of magnitude faster than TGF-α, ER, and AR. The β-turns were also observed to exchange faster for TGF-α, followed by EGF; whereas HB-EGF, ER, and AR were up to 100 orders of magnitude slower. At times, the kinetics was not sensitive enough to distinguish the rates of exchange for several secondary structural motifs within the same ligand. 2DCOS proved valuable in the establishment of the order of events in which these structural domains were exchanged with respect to one another, allowing further confidence. Therefore the combined analysis kinetics of H/D exchange and 2DCOS can be used to establish the order of events in the H/D exchange process.

H/D exchange studies monitored by FT-IR spectroscopy have been proven useful in the analysis of solvent accessibility at the structural motif level; but more importantly, hydrogen-bonding interaction was studied by determining the H/D exchange rates. The differences in exchange rates observed for these five ligands, within their side chains and secondary structural motifs, may be critical for receptor regulation. The next logical step in this work is to study the interaction between these ligands and the EGFR using ^{13}C-labeled ligands to allow the simultaneous study of both proteins within the complex.

REFERENCES

1. Riese, D. J., and D. F. Stern. 1998. Specificity within the EGF family/ErbB receptor family signaling network. *Bioessays.* 20:41–48.

2. Klein, P., D. Mattoon, M. A. Lemmon, and J. Schlessinger. 2004. A structure-based model for ligand binding and dimerization of EGF receptors. *Proc. Natl. Acad. Sci. USA.* 101:929–934.

3. Garrett, T. P., N. M. Mckern, M. Lou, T. C. Elleman, T. E. Adams, G. O. Lovrecz, H. J. Zhu, F. Walker, M. J. Frenkel, P. A. Hoyne, R. N. Jorissen, E. C. Nice, A. W. Burgess, and C. W. Ward. 2002. Crystal structure of a truncated epidermal growth factor receptor extracellular domain bound to transforming growth factor α. *Cell.* 110:763–773.

4. Ogiso, H., R. Ishitani, O. Nureki, S. Fukai, M. Yamanaka, J. H. Kim, K. Saito, A. Sakamoto, M. Inoue, M. Shirouzu, and S. Yokoyama. 2002. Crystal structure of the complex of human epidermal growth factor and receptor extracellular domains. *Cell.* 110:775–787.

5. Burgess, A. W., H. S. Cho, C. Eigenbrot, K. M. Ferguson, T. P. Garrett, D. J. Leahy, M. A. Lemmon, M. X. Sliwkowski, C. W. Ward, and S. Yokoyama. 2003. An open-and-shut case? Recent insights into the activation of EGF/ErbB receptors. *Mol. Cell.* 12:541–552.

6. Lenferink, A. E., E. J. van Zoelen, M. J. van Vugt, S. Grothe, W. van Rotterdam, M. L. van De Poll, and M. D. O'Connor-McCourt. 2000. Superagonist activation of ErbB-1 by EGF-related growth factors with enhanced association and dissociation rate constants. *J. Biol. Chem.* 275:26748–26753.

7. Davis-Fleischer, K. M., and G. E. Besner. 1998. Structure and function of heparin-binding EGF-like growth factor (HB-EGF). *Front. Biosci.* 3:d288–d299.

8. Freimann, S., I. Ben-Ami, A. Dantes, R. Ron-El, and A. Amsterdam. 2004. EGF-like factor epiregulin and amphiregulin expression is regulated by gonadotropins/cAMP in human ovarian follicular cells. *Biochem. Biophys. Res. Commun.* 324:829–834.

9. Higashiyama, S., K. Lau, G. E. Besner, J. A. Abraham, and M. Klagsbrun. 1992. Structure of heparin-binding EGF-like growth factor. Multiple forms, primary structure, and glycosylation of the mature protein. *J. Biol. Chem.* 267:6205–6212.

10. Shoyab, M., G. D. Plowman, V. L. McDonald, J. G. Bradley, and G. J. Todaro. 1989. Structure and function of human amphiregulin: a member of the epidermal growth factor family. *Science.* 243:1074–1076.

11. Louie, G. V., W. Yang, M. E. Bowman, and S. Choe. 1997. Crystal structure of the complex of diphtheria toxin with an extracellular fragment of its receptor. *Mol. Cell.* 1:67–78.

12. Montelione, G. T., K. Wuthrich, A. W. Burgess, E. C. Nice, G. Wagner, K. D. Gibson, and H. A. Scheraga. 1992. Solution structure of murine epidermal growth-factor determined by NMR-spectroscopy and refined by energy minimization with restraints. *Biochemistry.* 31:236–249.

13. Thorne, B. A., and G. D. Plowman. 1994. The heparin-binding domain of amphiregulin necessitates the precursor pro-region for growth factor secretion. *Mol. Cell.* 1:67–78.

14. Sato, K., T. Nakamura, M. Mizuguchi, K. Miura, M. Tada, T. Aizawa, T. Gomi, K. Miyamoto, and K. Kawano. 2003. Solution structure of epiregulin and the effect of its C-terminal domain for receptor binding affinity. *FEBS Lett.* 553:232–238.

15. Baba, I., S. Shirasawa, R. Iwamoto, K. Okumura, T. Tsunoda, M. Nishioka, K. Fukuyama, K. Yamamoto, E. Mekada, and T. Sasazuki. 2000. Involvement of deregulated epiregulin expression in tumorigenesis in vivo through activated Ki-Ras signaling pathway in human colon cancer cells. *Cancer Res.* 60:6886–6889.

16. Torring, N., F. D. Hansen, B. S. Sorensen, T. F. Orntoft, and E. Nexo. 2005. Increase in amphiregulin and epiregulin in prostate cancer xenograft after androgen deprivation-impact of specific HER1 inhibition. *Prostate.* 64:1–8.

17. Jones, J. T., R. W. Akita, and M. X. Sliwkowski. 1999. Binding specificities and affinities of egf domains for ErbB receptors. *FEBS Lett.* 447:227–231.

18. Derynck, R. R., M. E. Winkler, E. Y. Chen, and D. V. Goeddel. 2005. Human transforming growth factor-α: precursor structure and expression in *E. coli. Cell.* 38:287–297.

19. Alwan, H. A., E. J. van Zoelen, and J. E. M. van Leeuwen. 2003. Ligand-induced lysosomal epidermal growth factor receptor (EGFR) degradation is preceded by proteosome-dependent EGFR de-ubiquitination. *J. Biol. Chem.* 278:35781–35790.

20. Groenen, L. C., E. C. Nice, and A. W. Burgess. 1994. Structure-function relationships for the EGF/TGF-α family of mitogens. *Growth Factors.* 11:235–257.

21. Carpenter, G., and S. Cohen. 1990. Epidermal growth-factor. *J. Biol. Chem.* 265:7709–7712.

22. Kohda, D., N. Go, K. Hayashi, and F. Inagaki. 1988. Tertiary structure of mouse epidermal growth factor determined by two-dimensional 1H NMR. *J. Biochem. (Tokyo).* 103:741–743.

23. Kohda, D., C. Kodama, R. Kase, H. Nomoto, K. Hayashi, and F. Inagaki. 1988. A comparative 1H NMR study of mouse α (1–53) and β (2–53) epidermal growth factors. *Biochem. Int.* 16:647–654.

24. Kohda, D., and F. Inagaki. 1988. Complete sequence specific 1H NMR resonance assignments for mouse epidermal growth factor. *J. Biochem. (Tokyo).* 103:554–571.

25. Montelione, G. T., M. E. Winkler, L. E. Burton, E. Rinderknecht, M. B. Sporn, and G. Wagner. 1989. Sequence-specific 1H-NMR assignments and identification of two small antiparallel β-sheets in the solution structure of recombinant human transforming growth factor α. *Proc. Natl. Acad. Sci. USA.* 86:1519–1523.

26. Kline, T. P., F. K. Brown, S. C. Brown, P. W. Jeffs, K. D. Kopple, and L. Mueller. 1990. Solution structures of human transforming growth factor-α derived from H-1-NMR data. *Biochemistry.* 29:7805–7813.

27. Harvey, T. S., A. J. Wilkinson, M. J. Tappin, R. M. Cooke, and I. D. Campbell. 1991. The solution structure of human transforming growth factor-α. *Eur. J. Biochem.* 198:555–562.

28. Kohda, D., T. Sawada, and F. Inagaki. 1991. Characterization of pH titration shifts for all the nonlabile proton resonances in a protein by two-dimensional NMR: the case of mouse epidermal growth factor. *Biochemistry.* 30:4896–4900.

29. Kohda, D., and F. Inagaki. 1992. 3-Dimensional nuclear-magnetic-resonance structures of mouse epidermal growth-factor in acidic and physiological pH solutions. *Biochemistry.* 31:11928–11939.

30. Moy, F. J., Y. C. Li, P. Rauenbuehler, M. E. Winkler, H. A. Scheraga, and G. T. Montelione. 1993. Solution structure of human type-α transforming growth-factor determined by heteronuclear NMR-spectroscopy and refined by energy minimization with restraints. *Biochemistry.* 32:7334–7353.

31. Li, Y. C., and G. T. Montelione. 1995. Human type-α transforming growth-factor undergoes slow conformational exchange between multiple backbone conformations as characterized by N-15 relaxation measurements. *Biochemistry.* 34:2408–2423.

32. Fadel, A. R., D. Q. Jin, G. T. Montelione, and R. M. Levy. 1995. Crankshaft motions of the polypeptide backbone in molecular dynamics simulations of human type α transforming growth factor. *J. Biomol. NMR.* 6:221–226.

33. Stein, R. A., and J. V. Staros. 2000. Evolutionary analysis of the ErbB receptor and ligand families. *J. Mol. Evol.* 50:397–412.

34. Kabsch, W., and C. Sanders. 1983. Dictionary of protein secondary structure: pattern recognition of hydrogen-bonded and geometrical features. *Biopolymers.* 22:2577–2637.

35. Chang, J.-Y., and L. Li. 2002. The disulfide structure of denatured epidermal growth factor: preparation of scrambled disulfide isomers. *J. Protein Chem.* 21:203–213.

36. DeWitt, A., T. Iida, H. Y. Lam, V. Hill, H. S. Wiley, and D. A. Lauffenburger. 2002. Affinity regulates spatial range of EGF receptor autocrine ligand binding. *Dev. Biol.* 250:305–316.

37. Neelam, B., A. Richter, S. G. Chamberlin, S. M. Puddicombe, L. Wood, M. B. Murrray, K. Nandagopal, S. K. Niyogi, and D. Davies. 1998. Structure-function studies of ligand-induced epidermal growth factor receptor dimerization. *Biochemistry.* 37:4884–4891.

38. Wigens, M., T. Wama, H. van Ingen, C. Stortelers, J. E. M. van Leeuwen, E. J. van Zoelen, and G. W. Vuister. 2003. Structural analysis of an epidermal growth factor/transforming growth factor-α chimera with unique ErbB binding specificity. *J. Biol. Chem.* 278:39114–39123.

39. Holladay, L. A., C. R. Savage, S. Cohen, and D. Puett. 1976. Conformation and unfolding thermodynamics of epidermal growth and derivatives. *Biochemistry.* 15:2624–2633.

40. Acha, V., J. M. Ruysschaert, and E. Goormaghtigh. 2001. Stacks of close to 100 phospholipid bilayers fully accessible to proteins—an

ATR-FTIR-based chemometric analysis on hydrated phospholipid films. *Anal. Chim. Acta.* 435:215–226.

41. Goormaghtigh, E., H. H. J. deJongh, and J. M. Ruysschaert. 1996. Relevance of protein thin films prepared for attenuated total reflection Fourier transform infrared spectroscopy: significance of the pH. *Appl. Spectrosc.* 50:1519–1527.

42. Ortiz, M., Z. Sanoguet, H. Hu, W. J. Chazin, C. McMurray, J. L. Salisbury, and B. Pastrana-Rios. 2005. Dynamics of hydrogen-deuterium exchange in *Chlamydomonas* centrin. *Biochemistry.* 44: 2409–2418.

43. Raussens, V., J. M. Ruysschaert, and E. Goormaghtigh. 2004. Analysis of 1H/2H exchange kinetics using model infrared spectra. *Appl. Spectrosc.* 58:68–82.

44. Vigano, C., M. Smeyers, V. Raussens, F. Scheirlinckx, J. M. Ruysschaert, and E. Goormaghtigh. 2004. Hydrogen-deuterium exchange in membrane proteins monitored by IR spectroscopy: a new tool to resolve protein structure and dynamics. *Biopolymers.* 74:19–26.

45. Arrondo, J. L. R., A. Muga, J. Castresana, and F. M. Goñi. 1993. Quantitative studies of the structure of proteins in solution by Fourier-transform infrared spectroscopy. *Prog. Biophys. Mol. Biol.* 59:23–56.

46. Goormaghtigh, E., V. Raussens, and J. M. Ruysschaert. 1999. Attenuated total reflection infrared spectroscopy of proteins and lipids in biological membranes. *Biochim. Biophys. Acta.* 1422:105–185.

47. Nabet, A., and M. Pézolet. 1997. Two-dimensional FT-IR spectroscopy: a powerful method to study the secondary structure of proteins using H-D exchange. *Appl. Spectrosc.* 51:466–469.

48. Graff, D. K., B. Pastrana-Rios, S. Y. Venyaminov, and F. G. Prendergast. 1997. The effects of chain length and thermal denaturation on helix-forming peptides: a mode-specific analysis using 2D FT-IR. *J. Am. Chem. Soc.* 119:11282–11294.

49. Krimm, S., and J. Bandekar. 1986. Vibrational spectroscopy and conformation of peptides, polypeptides, and proteins. *Adv. Protein Chem.* 38:181–364.

50. Arrondo, J. L., and F. M. Goñi. 1999. Structure and dynamics of membrane proteins as studied by infrared spectroscopy. *Prog. Biophys. Mol. Biol.* 72:367–405.

51. Pastrana-Rios, B. 2001. Mechanism of unfolding of a model helical peptide. *Biochemistry.* 40:9074–9081.

52. Pastrana-Rios, B., W. Ocana, M. Rios, G. L. Vargas, G. Ysa, G. Poynter, J. Tapia, and J. L. Salisbury. 2002. Centrin: its secondary structure in the presence and absence of cations. *Biochemistry.* 41:6911–6919.

53. Chirgadze, Y. N., O. V. Fedorov, and N. P. Trushina. 1975. Estimation of amino acid residue side-chain absorption in the infrared spectra of protein solutions in heavy water. *Biopolymers.* 14:679–694.

54. Venyaminov, S. Y., and N. N. Kalnin. 1990. Quantitative IR spectrophotometry of peptide compounds in water (H_2O) solutions. 1. Spectral parameters of amino-acid residue absorption-bands. *Biopolymers.* 30: 1243–1257.

55. Venyaminov, S. Y., and N. N. Kalnin. 1990. Quantitative IR spectrophotometry of peptide compounds in water (H_2O) solutions. 2. Amide absorption-bands of polypeptides and fibrous proteins in α-coil, β-coil, and random coil conformations. *Biopolymers.* 30:1259–1271.

56. Meskers, S., J. M. Ruysschaert, and E. Goormaghtigh. 1999. Hydrogen-deuterium exchange of streptavidin and its complex with biotin studied by 2D-attenuated total reflection Fourier transform infrared spectroscopy. *J. Am. Chem. Soc.* 121:5115–5122.

57. Noda, I., A. E. Dowrey, C. Marcott, G. M. Story, and Y. Ozaki. 2000. Generalized two-dimensional correlation spectroscopy. *Appl. Spectrosc.* 54:236A–248A.

58. Ferguson, K. M., M. B. Berger, J. M. Mendrola, C. Hyun-Soo, D. J. Leahy, and M. A. Lemmon. 2003. EGF activates its receptor by removing interactions that autoinhibit ectodomain dimerization. *Mol. Cell.* 11:507–517.

59. ExPASy - UniProt Knowledgebase. 2007. Swiss-Prot and TrEMBL. http://expasy.org/sprot/.

60. Kyte, J., and R. Doolittle. 1982. A simple method for displaying the hydropathic character of a protein. *J. Mol. Biol.* 157:105–132.